10

# Photoactive Cu-Containing $ZnO-ZnAl_2O_4$ nanocomposites

© A. Tinku[1], A.A. Shelemanov[1], S.K. Evstropiev[1,2,3], N.V. Nikonorov[1], A.V. Karavaeva[4], V.M. Kiselev[3]

[1] ITMO University,
197101 St. Petersburg, Russia
[2] St. Petersburg State Technological Institute (Technical University),
190013 St. Petersburg, Russia
[3] „Vavilov State Optical Institute“,
192171 St. Petersburg, Russia
[4] St. Petersburg State Chemical Pharmaceutical Academy,
197022 St. Petersburg, Russia

e-mail: artem.tinku@mail.ru

*Received February 15, 2022*
*Revised July 05, 2022*
*Accepted July 15, 2022*

Photoactive Cu-containing ZnO-ZnAl2O3 nanocomposites were synthesized by the polymer-salt method. To study the structure and properties of materials, the methods of luminescent spectroscopy and X-ray phase analysis were used. It has been shown that the resulting nanocomposites are capable of photogeneration of singlet oxygen under the action of UV and blue light. The synthesized materials consist of nanosized hexagonal ZnO crystals and cubic $ZnAl_2O_4$ crystals doped with Cu. The study of luminescent properties showed that nanocomposites can be used as down-converters of light that convert radiation from the UV-C range to UV-A and the visible spectral range.

**Keywords:** singlet oxygen, nanoparticle, luminescence, ZnO, $ZnAl_2O_4$.

DOI: 10.21883/EOS.2022.10.54869.3275-22

## 1. Introduction

It is well known that one of the most effective oxide photocatalysts and solid bactericidal media are materials based on zinc oxide [1–5]. Particularly effective are ZnO-based heterostructure composites containing various semiconductor and metal nanoparticles [5–10]. Photogeneration of reactive oxygen intermediates (singlet oxygen [5,9,11,12], hydroxyl [13] and peroxide [6,13] radicals) plays a key role in photocatalytic processes and antibacterial activity of materials. The characteristics of the exciting radiation, the structure and morphology of materials have a strong influence on the photogeneration of reactive oxygen intermediates [1,12–14]. Highly dispersed materials, characterized by high specific surface area, show a higher ability to photogenerate reactive oxygen intermediates and demonstrate higher photocatalytic properties and antibacterial activity compared to their macroscopic counterparts [1]. Particle size reduction and material morphology optimization are used to increase photocatalytic and bactericidal properties [1,2,5,9,10,15,16]. It is known [5,9,17] that the size of crystals in two-component oxide composites is smaller than in one-component analogues synthesized under similar conditions. This phenomenon is used to reduce the size of crystals in photoactive materials and improve their characteristics [5,9].

In [5,9,11] this particle size reduction method was used to synthesize highly dispersed photoactive materials ZnO-$Al_2O_3$ [11], $ZnO-SnO_2$ [5] and $ZnO-MgO-Ag$ [9]. The temperature-time synthesis conditions used in [5,9,11] ensured the simultaneous formation of two different crystalline phases ($ZnO + \gamma$-$Al_2O_3$ [ ]11; $ZnO + SnO_2$ [5]; $ZnO + MgO$ [9]) in the material structure without their chemical interaction.

In this work, we used elevated synthesis temperatures compared to those used in [5,9,11] to form nanocomposites consisting of a mixture of small and densely-packed hexagonal ZnO crystals and cubic spinel crystals $ZnAl_2O_4$.

The photocatalytic and antibacterial properties of zinc oxide are well known [3–10,15,16]. The use of $ZnAl_2O_4$ as a photocatalyst material has also been described in [18–27]. It was shown in [27] that the photocatalytic properties of $ZnAl_2O_4$ increase with the introduction of copper additives in the composition of the material.

Cu-containing nanocomposites of the $ZnO-Al_2O_3$ system are characterized by high photocatalytic and antibacterial properties, are effective catalysts for the conversion of $CO_2$ into various organic compounds, and can be used as materials for sensors [7,24,27,28]. It was shown in [7] that Cu-containing nanocomposites based on ZnO demonstrate high antibacterial activity, which increases with increasing copper content in the material.

The purpose of this work was the synthesis and study of the structure, luminescent properties, and the ability to photogenerate reactive singlet oxygen by Cu-containing $ZnO-ZnAl_2O_4$ nanocomposites.

## 2. Materials and methods

Aqueous solutions of $Zn(NO_3)_2$, $Al(NO_3)_3$, $CuSO_4$ were used as initial materials in the work. Sample weights

Chemical composition of composites and average size of ZnO crystals in their structure

| Sample number | CuO addition, mass.% | | | Average size of ZnO crystals in composites, nm |
|---|---|---|---|---|
| | ZnO | $ZnAl_2O_4$ | CuO, over 100% | |
| *1* | 79.43 | 20.57 | 0.74 | 12.5 |
| *2* | 79.43 | 20.57 | 0.56 | 8.4 |
| *3* | 79.43 | 20.57 | 0.38 | 8.2 |
| *4* | 79.43 | 20.57 | 0.18 | 7.6 |
| *5* | 79.43 | 20.57 | 0.08 | 8.3 |

for metal salts were dissolved in a 50% solution of isopropyl alcohol at room temperature and mixed with an aqueous solution of polyvinyl-pyrrolidone (PVP) (K30, $M_w = 25000-35000$ g/mol). The resulting mixture was stirred with a magnetic stirrer for 30 min. The solutions were dried in a drying oven at temperature of 75°C.The polymer-salt composites obtained as a result of drying were subjected to heat treatment in an electric furnace at temperature of 680°C for 2 h. The used temperature-time mode of heat treatment ensured the complete decomposition of PVP and metal salts and the formation of an oxide composite material [5,9]. In the present work, composites with variable copper content were synthesized. The chemical compositions of the obtained oxide composites are given in the table.

X-ray diffraction analysis was used to study the crystal structure of the resulting composites. The studies were performed using Rigaku Ultima IV X-ray diffractometer. The average size $d$ of ZnO crystals was calculated from the obtained data using the Scherrer formula.

Powder photoluminescence measurements in the UV and visible spectral ranges were performed by Perkin Elmer LS-50B fluorescent spectrophotometer. Under the action of external radiation, singlet oxygen exhibits characteristic luminescence in the near-IR region of the spectrum ($\lambda_{max} = 1270$ nm) [29]. To study the photogeneration of singlet oxygen by nanocomposites, one used the experimental apparatus described in [30]. LEDs were used to excite the luminescence. series HPR40E-50UV were used; ($\lambda_{max} = 370$ nm; power density 0.35 W/cm$^2$) and ($\lambda_{max} = 405$ nm; power density 0.90 W/cm$^2$).

## 3. Experimental results and discussion

### 3.1. Crystal structure and morphology of composites

X-ray diffraction analysis of nanocomposites showed the presence in them of two crystalline phases i.e. hexagonal ZnO crystals with a wurtzite structure and cubic crystals of spinel $ZnAl_2O_4$ (Fig. 1). The intensity of ZnO peaks on X-ray diffraction patterns is significantly higher than that of spinel crystals, which is determined by the significantly

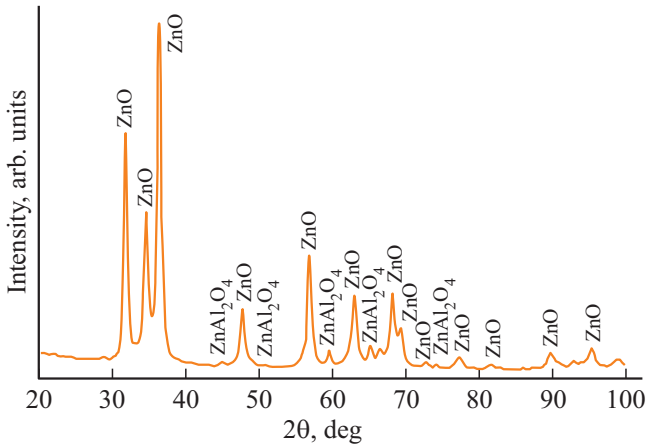


**Figure 1.** X-ray diffraction pattern of the composite *5*.

higher concentration of this component in nanocomposites (table). It should be noted that the peaks of $\gamma$-$Al_2O_3$ crystals, which appeared on the x-ray diffraction patterns given in [11] for $ZnO-Al_2O_3$ composites, formed at lower temperatures (550°C).

In addition, there peaks of copper compounds absent on the X-ray diffraction patterns. This may be due to both the relatively low concentration of this component in the materials and the possible incorporation of copper ions into the crystal lattices of zinc-containing crystals. The values of the crystal lattice parameters of ZnO crystals in nanocomposites, calculated on the basis of XPA data, are somewhat smaller than the data given in the review [31] for zinc oxide crystals. Thus, the values of the lattice parameters of hexagonal ZnO crystals in the *3* composite were: $a = 3.2444(6)$ Å; $c = 5.1938(12)$ Å, while the lattice parameters of ZnO according to [31] are: $a = 3.2475-3.2501$ Å; $c = 5.2042-5.2075$ Å). The observed smaller values of the ZnO lattice parameters can be explained by the incorporation of $Cu^{2+}$ ions into it, which have somewhat smaller size compared to $Zn^{2+}$ ions (ionic radii of $Cu^{2+}$ and $Zn^{2+}$ are 0.57 and 0.60 Å respectively [32]). It is known that ions $Cu^{2+}$ easily replace $Zn^{2+}$ in the structure of crystals, causing a slight contraction of the lattice cell of crystals [33].

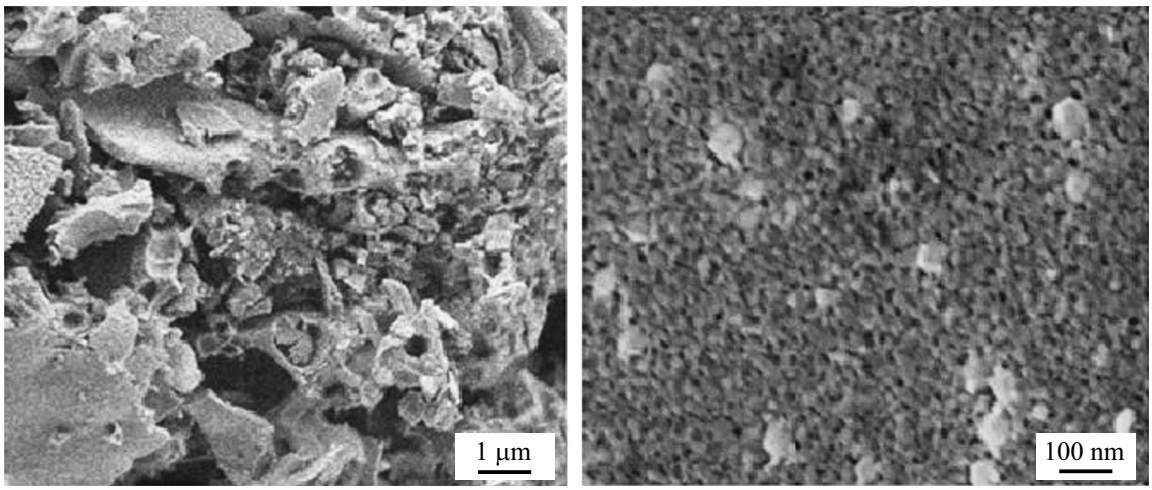


**Figure 2.** Electron microscopic images (at various magnifications) of the composite *3*.

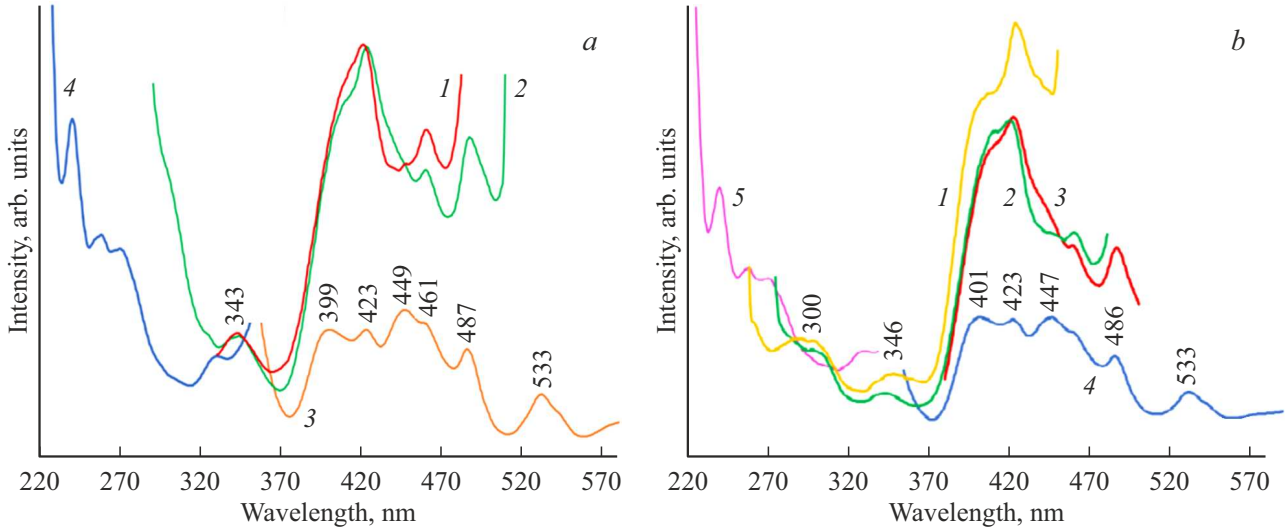


**Figure 3.** Photoluminescence and luminescence excitation spectra of the sample *1* (*a*, curves *1–3* and curve *4*, respectively) and the sample *5* (*b* , curves *1–4* and curve *5* respectively). Luminescence excitation wavelength 257 (curves *1*); 270 (curves *2*); 330 (Fig. *a*, curve *3*), 350 (Fig. *b*, curve *3*), 390 nm (Fig. *b*, curve *4*). Recording wavelength at measuring excitation spectra 390 nm

This corresponds to the data of the work [34] that materials of the ZnO–CuO system with a copper content of less than 15% are characterized by a single-phase crystal structure of Cu $Zn_{1-x}O$ like a wurtzite-type. Also note that it was shown in [35,36] that silver ions can be incorporated into the crystal lattice of zinc oxide and deform it somewhat, which is affected in the change in the crystal lattice parameters.

On the basis of the experimental data obtained, it can be concluded that the effect of copper additions on the size of the formed ZnO crystals is practically not manifested (table). When the content of CuO additives changes from 0.08 to 0.56 mass.%, the size of ZnO crystals does not change, and a slight increase in the size of these crystals is observed only in the sample *1* with the maximum content (0.74 mass.%) of copper additives. The observed weak effect of CuO additives on the size of zinc oxide crystals can be explained by their low content in the synthesized composites.

Peaks of cubic spinel $ZnAl_2O_4$ crystals (JCPDS № 05-0669) are observed in X-ray diffraction patterns of all composites. The presence of these crystals in the structure of composites is consistent with the literature data [27,37,38], indicating that the use of various liquid-phase methods (codeposition [27], sol-gel [38], polymer-salt method [37]) provides the formation of $ZnAl_2O_4$ spinel crystals at relatively lower temperatures ($T > 550°C$, jcite15) compared to conventional solid-phase synthesis (1300°C [39]). Figure 2 shows electron microscopic images of the composite *3*. It can be seen that the powder consists of micron-sized

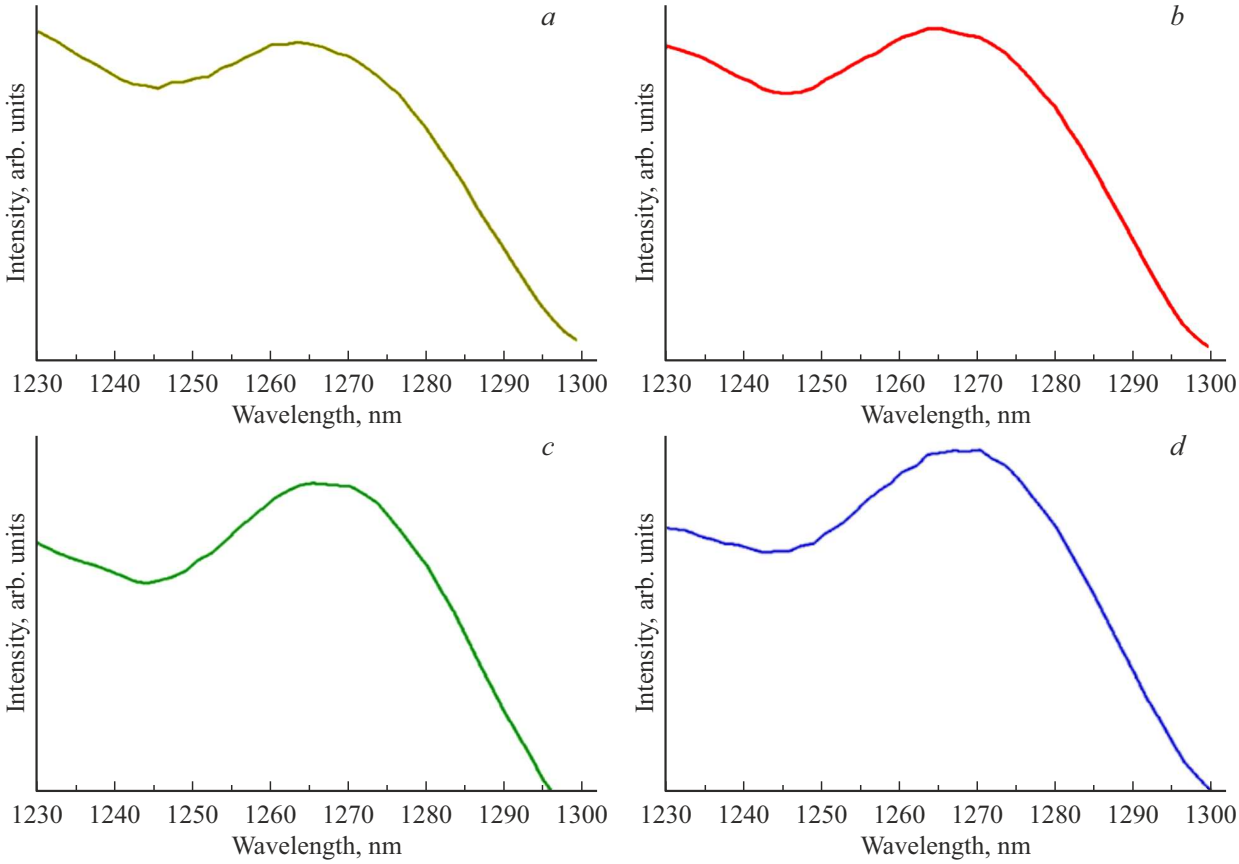


**Figure 4.** ($\lambda_{exc} = 405$ nm) in the near-IR region of the spectrum of Cu-containing $ZnO/ZnAl_2O_4$ composites with different copper contents. CuO content, wt/%: 0.08 (*a*); 0.18 (*b*); 0.56 (*c*); 0.74 (*d*).

particles (Fig. 2, *a*), has a porous structure, and consists of small ($\sim 10-15$ nm) nanoparticles (Fig. 2, *b*). This morphology provides a high specific surface area of the material, which, in turn, contributes to its ability to photogenerate reactive oxygen intermediates.

### 3.2. Photoluminescence

The photoluminescence spectra of the composites exhibit numerous emission peaks with maxima at 343, 399, 423, 440, 461, 487, and 533 nm (Fig. 3). Two main peaks are often observed in materials based on zinc oxide: an exciton peak near the absorption edge of ZnO (380–420 nm) and a broad emission band in the visible part of the spectrum, which is the result of the superimposition of several luminescence bands and is due to various defects in the crystalline structures of zinc oxide [40]. Thus, in the spectra of thin ZnO films, luminescence bands associated with defects in ZnO crystals were observed in [41] at 399, 417, 438, 453, 467 nm and in the green region of the spectrum. The mechanisms of ZnO luminescence in the visible part of the spectrum were considered in detail in [42].

The introduction of copper into the structure of ZnO crystals leads to a decrease in the band gap [36] and several emission peaks are also observed in the photoluminescence spectra of these materials [43,44]. In the photoluminescence spectrum of the $CuO-ZnO-ZnAl_2O_4$ composite, emission bands with maxima at 411, 433, 459, and 492 nm [44] were observed.

The presence in the luminescence spectra of bands associated with intrinsic defects of zinc oxide crystals is an additional confirmation of the incorporation of copper ions into the structure of these crystals. Also, note that the presence of intrinsic defects in the ZnO structure can enhance the photocatalytic properties of materials [44–47].

Thus, based on a comparison of the experimentally measured luminescence spectra (Fig. 3) with the literature data, one can conclude that the luminescence in the blue and green parts of the spectrum in the composites synthesized by us is determined by various defects in the crystal structure of zinc-containing oxide crystals.

The luminescence band with a maximum $\lambda_{max} = 343$ nm can be associated with the emission of $ZnAl_2O_4$ crystals. According to ([24,37,48–50]), the values of the band gap of these crystals, obtained by various methods, vary over a wide range : from 3.9 to more than 6.0 eV. However, it was shown in [39,51] that $ZnAl_2O_4$ can be used as a light-emitting luminophor under the action of hard UV radiation ($\lambda_{exc} < 200$ nm), in the UV-C spectral range, which indicates that $ZnAl_2O_4$ is a wide-band gap material.

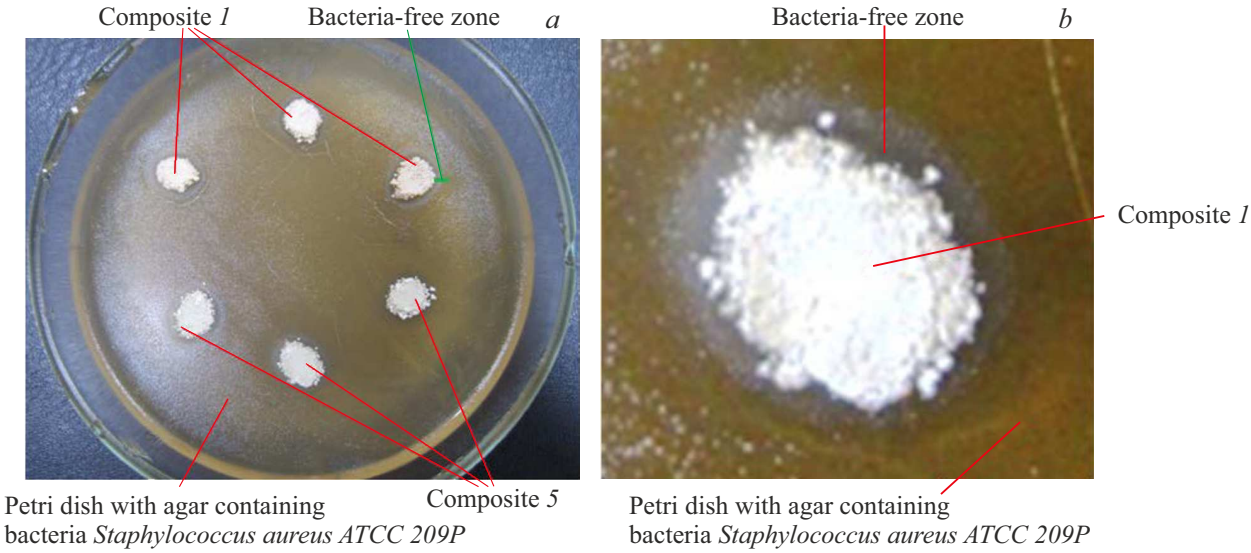


**Figure 5.** Photographs illustrating the antibacterial activity of the composite *1*.

It should be noted that emission with $\lambda_{max} = 343$ nm is observed upon excitation with UV radiation ($\lambda_{exc} = 240$ nm) (curve *5*, Fig. 3, *b*). Thus, the obtained nanocomposites can play the role of down converters that convert radiation from the UV-C spectral range to UV-A and the visible part of the spectrum.

### 3.3. Photogeneration of singlet oxygen

Experiments have shown that the synthesized materials are capable of photogeneration of singlet oxygen both under the action of near UV radiation and blue light. Fig. 4 shows the photoluminescence spectra of Cu-containing $ZnO/ZnAl_2O_4$ composites in the near IR region of the spectrum. On all spectra,one can clearly see the luminescence band characteristic of singlet oxygen with a maximum $\lambda_{max} = 1270$ nm.

It can be seen from Fig. 4 that an increase in the copper content leads to some increasing in the intensity of the singlet oxygen luminescence band.

### 3.4. Antibacterial activity of composites

Fig. 5, *a* shows a photograph of a Petri dish with agar containing bacteria *Staphylococcus aureus ATCC 209P,* with samples of composites *1* and *5*. It can be seen that a zone of a slightly darker shade, free from bacteria, formed around each of the samples. In fig. 5, *b* the segment of this photograph is shown on enlarged scale. Thus, the experiments showed that the obtained nanocomposites have antibacterial activity against gram-positive bacteria. No significant difference in the width of the bacteria-free zone was observed in the experiments. This may be related to the incorporation of copper ions into the structure of oxide crystals in the nanocomposites obtained by us.

At the same time, the composites showed no antibacterial activity against a representative of gram-negative bacteria *Escherichia coli ATCC 25922.* The reasons for the observed difference in the antibacterial activity of the obtained composites against various bacteria require additional study.

## 4. Conclusion

Cu-containing composites $ZnO-ZnAl_2O_4$ were synthesized by the polymer-salt method. The structure of the obtained composites includes hexagonal ZnO nanocrystals (size 7.6–12.5 nm) and cubic spinel crystals. Copper ions introduced into the composition of the initial solutions are introduced into the structure of zinc-containing crystals during heat treatment, causing their deformation.

In the photoluminescence spectra of the composites, numerous emission bands are observed in the near UV part of the spectrum and in the visible one. Thus, the obtained nanocomposites can play the role of down converters that convert radiation from the UV-C spectral range to UV-A and the visible part of the spectrum.

The synthesized Cu-containing $ZnO-ZnAl_2O_4$ composites demonstrate the ability to generate singlet oxygen under the action of near-UV band radiation and blue light. The introduction of copper into the composition of materials, as well as the partial replacement of ZnO with $ZnAl_2O_4$ crystals, enhances the ability to photogenerate the singlet oxygen. Experiments have shown that nanocomposites have antibacterial activity against gram-positive bacteria.

### Acknowledgments

This study was supported by the Russian Science Foundation (grant № 20-19-00559).

The authors are grateful to Kuzmenko N.K. and Candidate of geological and mineralogical sciences Sadovnichy R.V. for assistance in performance of X-ray diffraction analysis of materials.

### Conflict of interest

The authors declare that they have no conflict of interest.

## References

[1] K.R. Raghupathi, R.T. Koodali, A.C. Manna. Langmuir. **27** (7), 4028 (2011). DOI: 10.1021/la104825u.
[2] K. Qi, Cheng B., J. Yu, W. Ho. J. Alloys Comp, **727**, 792 (2017). DOI: 10.1016/j.jallcom.2017.08.142.
[3] J. Theerthagiri, S. Salla, R.A. Senthil, P. Nithyadharseni, A. Madankumar, P. Arunachalam, T. Maiyalagan, H.-S. Ki. Nanotechnology, **30** (39), 392001 (2019). DOI: 10.1088/1361-6528/ab268a.
[4] F. Lin, B. Cojocaru, C.-L. Chou, C.A. Cadigan, Y. Ji, D. Nordlund, T.-C. Weng, Z. Zheng, V.I. Pérvulescu, R.M. Richards. ChemCatChem, **5** (12), 3841 (2013). DOI: 10.1002/cctc.201300440.
[5] S.K. Evstropiev, A.V. Karavaeva, M.A. Petrova, N.V. Nikonorov, V.N. Vasilyev, L.L. Lesnykh, K.V. Dukelskii. Mater. Today Comm., **21**, 100628 (2019). DOI: 10.1016/j.mtcomm.2019.100628.
[6] S.K. Sinha, T. Rakshit, S.K. Ray, I. Manna. Appl. Surf. Sci., **257** (24), 10551 (2012).
[7] L. Zhu, H. Li, Z. Liu, P. Xia, Y. Xie, D. Xiong. J. Phys. Chem., **122** (17), 9531 (2018). DOI: 10.1021/acs.jpcc.8b01933.
[8] L. Shi, L. Liang, J. Ma, J. Sun. Superlattices and Microstructures, **62**, 128 (2013). DOI: 10.1016/j.spmi.2013.07.013.
[9] A.A. Shelemanov, S.K. Evstropiev, A.V. Karavaeva, N.V. Nikonorov, V.N. Vasilyev, Y.F. Podruhin, V.M. Kiselev. Mater. Chem. Phys., **276**, 125204 (2022). DOI: 10.1016/j.matchemphys.2021.125204.
[10] Z. Cheng, S. Zhao, L. Han. Nanoscale, **10**, 6892(2018). DOI: 10.1039/c7nr09683f.
[11] S. Maslennikov, S. Evstropiev, I. Sochnikov, A. Karavaeva, K. Dukelskii, V. Gridchin. Opt. Engineering, **58** (7), 077105(2019). DOI: 10.1117/1.OE.58.7.077105.
[12] Y. Li, W. Zhang, J. Niu, Y. Chen. ACS Nano, **6** (6), 5164 (2012). DOI: 10.1021/nn300934k.
[13] F. Vatansever, W.C.M.A. de Melo, P. Avci, D. Vecchio, M. Sadasivam, A. Gupta, R. Chandran, M. Karimi, N.A. Parizotto, R. Yin, G.P. Tegos, M.R. Hamblin. FEMS Microbiol., **37**, 955 (2013). DOI: 10.1111/1574-6976.12026.
[14] R. Li, L. Zhang, P. Wang. Nanoscale, **7**, 17167 (2015). DOI: 10.1039/c5nr04870b.
[15] W.S. Chiu, P.S. Khiew, M. Cloke, D. Isa, T.K. Tan, S. Radiman, R. Abd-Shukor, M.A. Abd. Hamid, N.M. Huang, H.N. Lim, C.H. Chia. Engineering J., **158**, 345 (2010).
[16] S. Wang, P. Kuang, B. Cheng, J. Yu, C. Jiang. J. Alloys Comp., **741**, 622 (2018).
[17] R.C. Bradt, S.L. Burkett, *Ceramic Microstructures: Control at the Atomic Level* (Springer Science & Business Media, New York, 1998), p. 339.
[18] E.L. Foletto, S. Battiston, J.M. Simões, M.M. Bassaco, L.S.F. Pereira, É.M.M. Flores, E.I. Müller. Microporous and Mesoporous Materials, **163**, 29 (2012).
[19] C.G. Anchieta, D. Sallet, E.L. Foletto, S.S. da Silva, O. Chiavone-Filho, C.A.O. do Nascimento. Ceram. Int., **40**, 4173 (2014).
[20] S. Battiston, C. Rigo, E. Severo, M. Mazutti, R.C. Kuhn, A. Gündel, E.L. Foletto. Mater. Research, **17** (3), 734 (2014). DOI: 10.1590/S1516-14392014005000073.
[21] M. Zawadzki, W. Staszak, F.E. López-Suárez, M.J. Illán-Gómez, A. Bueno-López. Appl. Catalysis A: General, **371** (1), 92 (2009).
[22] X. Zhao, L. Wang, X. Xu, X. Lei, S. Xu, F. Zhang. AIChE Journal, **58** (2), 573 (2012).
[23] A. Chaudhary, A. Mohammad, S.M. Mobin. Materials Science and Engineering, **227**, 136 (2018).
[24] M. Shahmirzaee, M.S. Afarani, A.M. Arabi, A.I. Nejhad. Res. Chem. Intermed., **43**, 321 (2017).
[25] X. Yuan, X. Cheng, Q. Jing, J. Niu, D. Peng, Z. Feng, X. Wu. Materials (Basel), **11** (9), 1624 (2018).
[26] L. Zhang, J. Yan, M. Zhou, Y. Yang, Y.-N. Liu. Appl. Surf. Sci, **268**, 237 (2013).
[27] F.Z. Akika, M. Benamira, H. Lahmar, M. Trari, I. Avramova, Ş. Suzer // Surface and Interfaces. 2020. V. 18. p. 100406.
[28] Xian-ji Guo, Li-min Li, Shu-min Liu, Gai-ling Bao, Wenhua Hou. mJ. Fuel Chem. and Technol, **35** (3), 329 (2007).
[29] A.A. Krasnovsky, R.V. Ambartzumian. Chem. Phys. Lett., **400**, 531 (2004).
[30] V.M. Kiselev, I.M. Kislyakov, A.N. Burchinov. Opt. Spectrosc., **120** (4), 520 (2016).
[31] H. Morkoş, Ü. Özgür. Materials and Device Technology, 1 (2009).
[32] R.D. Shannon, *Revised effective ionic radii and systematic studies of interatomic distances in halides and chalcogenides* (Acta Cryst., 1976), p. 751–767.
[33] A.R. Lim. AIP Advances. **9**, 105115 (2019).
[34] D.M. Fernandes, R. Silva, A.A. Winkler Hechenleitner, E. Radovanovic, M.A. Custódio Melo, E.A. Gómez Pineda. Mater. Chem. Phys., **115**, 110 (2009).
[35] V.M. Volynkin, D.P. Danilovich, S.K. Evstropiev, K.V. Dukelsky, K.Yu. Senchik, R.V. Sadovnichy, V.M. Kiselev, I V. Bagrov, A.S. Saratovsky, N.V. Nikonorov, P.V. Bezborodkin. Optika i spektroskopiya**129** (5), 642?649 (2021) (in Russian).
[36] T. Chitradevi, A.J. Lenus, N.V. Jaya. Mater. Research Express, **7**, 1 (2020)
[37] S.-F. Wang, G.-Z. Sub, L.-M. Fang, L. Lei, X. Xiang, X.-T Zu. Sci. Rep., **5**, 12849 (2015).
[38] F. Davar, M. Salavati-Niasari. J. Alloys Comp., **509** (5), 2487 (2011).
[39] H. Komitami, N. Sonoda, K. Hara. In: *Proceedings of the International Display Workshops* (IDW, 2020), p. 346–349.
[40] R.S. Zeferino, M.B. Flores, U. Pal. J. Appl. Phys. **109**, (2011).
[41] D. Das, P. Mondal. RSC Adv., **4**, 35735 (2014).
[42] P.A. Rodny, K.A. Chernenko, I.D. Venevtsev. Optika i spektroskopiya, **125** (3), 357−363 (2018). (in Russian). DOI: 10.21883/OS/2018/09/46551/141-18 [P.A. Rodnyi, K.A. Chernenko, I.D. Venevtsev, Opt. Spectr., **125** (3), 372–378 (2018)].
[43] B. Allabergenov, U. Shaislamov, H. Shim, M.-J. Lee, A. Matnazarov, B. Choi. Optical Materials Express, **7** (2), 494 (2017).

[44] M.A. Subhan, T. Ahmed, R. Awal, R. Makioka, H. Nakata, T.T. Pakkanen, M. Suvanto, B.M. Kim. J. Luminescence, **146**, 123 (2014).
[45] P. Wang, Z.Y. Wang, B.B. Huang, Y.D. Ma, Y.Y. Liu, X.Y. Zhang, Y. Dai. ACS Appl. Mater. Interfaces, **4**, 4024 (2012).
[46] X.H. Lu, G.M. Wang, S.L. Xie, J.Y. Shi, W. Li, Y.X. Tong, Y. Li. Chem. Commun., **48**, 7717 (2012).
[47] D.M. Hofmann, D. Pfisterer, J. Sann, B.K. Meyer, R. Tena-Zaera, V. Munoz-Sanjose, T. Frank, G. Pensl. Appl. Phys. A, **88**, 147 (2007)
[48] S.S. Sampath, D.G. Kanhere, R. Pandey. J. Phys: Condensed Matter, **11**, 3635 (1999).
[49] H. Dixit, N. Tandon, S. Cottenier, R. Saniz, D. Lamoen, B. Partoens, V. Van Speybrock, M. Waroquier. J. Physics, **13**, 234 (2011).
[50] T. Tangcharoen, J. T-Thrienprasert, C. Kongmark. J. Adv. Ceram., **8** (3), 352 (2019).
[51] T. Ishinaga, T. Iguchi, H. Kominami, K. Hara, M. Kitaura, A. Ohnishi. Physica Status Solidi, **12** (6), 797 (2015).